PCCP

Accepted Manuscript

ROYAL SOCIETY OF CHEMISTRY

www.rsc.org/pccp

The table of contents:

The encapsulation of anti-cancer drug, that should protect it during its transport, is energetically favored inside small boron nitride nanotubes.

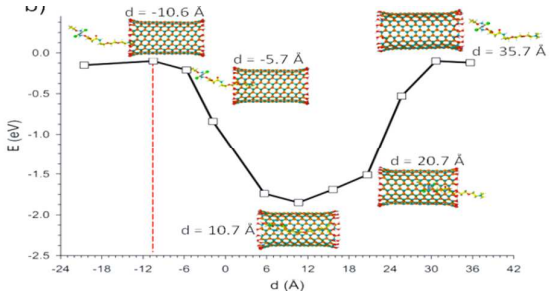

Journal Name

RSCPublishing

ARTICLE

Quantum study of boron nitride nanotubes functionalized with anticancer molecules

Cite this: DOI: 10.1039/x0xx00000x

Eric Duverger[1], Tijani Gharbi[2], Eric Delabrousse[2] and Fabien Picaud[2]

Received 00th January 2012,
Accepted 00th January 2012

DOI: 10.1039/x0xx00000x

www.rsc.org/

Full DFT-D2 calculations were investigated to study the interactions between single wall (10,10) boron nitride nanotubes (BNNTs) and different molecules, such as azomethine (C_2H_5N) and an anticancer agent (Pt(IV) complex) linked to an amino-derivative chain. The geometry of the (10,10) BNNT-azomethine and BNNT-amino derivative system was optimised by considering different molecular configurations on the inner and outer surfaces of the nanotube. Simulation results showed that the most stable physisorption state for both molecules was located inside the nanotube in a parallel configuration. We showed also that the molecular chemisorption was possible only when the azomethine was above two adjacent B and N atoms of a hexagon. The attachment of an azomethine plus a subsequent drug did not perturb the cycloaddition process. Moreover, all theoretical results showed that the therapeutic agent complex was not affected when it was attached onto BNNTs.

[1] Institut FEMTO-ST, 32 Avenue de l'Observatoire, 25044 Besançon, France.
[2] Laboratoire de Nanomédecine, Imagerie et Thérapeutique, Université Franche-Comté, Centre Hospitalier Universitaire de Besançon, 16 route de Gray, 25030 Besançon cedex, France.

Journal Name

RSCPublishing

ARTICLE

Introduction

Development of research focused on better ways to treat cancer is the consequence of the massive increase in the number of cancer cases. Nowadays, several treatment protocols, including surgery, radiation and chemotherapeutic drugs, are used successively or simultaneously to treat cancer and limit its invasion. Most current research is dedicated to targeting the diseased cells, thus avoiding the destruction of healthy cells and the development of treatment-induced side effects. Since the mid-1980s, the development of nanocarriers, incorporating both chemotherapeutic drugs and receptors specific to the target cells, is certainly the most promising strategy despite some drawbacks[1-8].

Indeed, the random nature of targeting makes the process and the correct release of the drug difficult to control. This lack of control could be at the origin of multiple drug resistances. To overcome this, nanocarriers can be programmed to actively bind to specific cells by using a targeting agent that interacts specifically with a receptor overexpressed on cancer cells. Nanocarriers are then constituted by ligands dedicated to recognition and by the internalised active drug treating the targeted cells. Several nanostructures were tested to achieve this goal, for example, aptamer-conjugated nanoparticles that target the specific antigen of prostate cancer cells and deliver docetaxel with success *in vivo*. Other nanomaterials are now used such as polymers, liposomes, micelles, carbon[9, 10] or gold nanocage in a wide variety of applications.

Drug encapsulation inside the nanostructure is challenging because it carries the drug without any chemical modification, but necessitates the control of its release near cancer cells. Boron nitride nanotubes (BNNTs) are promising alternative nanocarriers offering several advantages, such as a large inner volume enabling encapsulation of more drugs, different inner and outer surfaces, and generally with open ends allowing the drug to penetrate it if the energy interaction is favourable. Compared to carbon nanotubes (CNTs), BNNTs are wide bandgap semiconductors exhibiting high chemical stability with electronic properties independent of the nanotube diameter.[11, 12] Moreover, high-purity and high-quality BNNTs are inherently non-cytotoxic, unlike CNTs. BNNTs could thus be suitable for biomedical applications when their solubility and their biocompatibility is achieved by means of chemical functionalization.[13, 14] As for CNTs, both physisorption and chemisorption functionalization schemes were studied for BNNTs.[15-17] In case of physisorption of BNNTs with molecules, the π–π stacking between the two interacting units is preponderant.[15, 18-21] In case of chemisorption, the reactivity to treat van der Waals interactions optimised for several DFT T functionals. Mtube diameter.[22, 23] Moreover, Li et al. reported an inverted behaviour from chemisorption to physisorption as a function of the tube diameter for NH_3 molecules adsorbed onto BNNTs.[23]

In this paper, we aim to expand the domain of BNNTs for drug delivery applications. For this, we carried out a systematic study on the noncovalent and covalent functionalization of BNNTs with azomethine (C_2H_5N) and the azomethine derivative Pt molecule, i.e. a cancer-drug. We showed that using the density functional theory (DFT) including the semi-empirical van der Waals correction in the Grimme scheme, we described correctly both the strong chemisorption minima energy near the surface and the weak physisorption minima energy further away from the surface.[24-26] Platinum (Pt) complexes are drugs commonly used in cancer chemotherapy[27, 28]. They act by binding DNA and preventing its transcription and replication leading to cellular apoptosis[29]. Nevertheless, cells develop different mechanism of resistance to this drug; one solution to overcome this is to use Pt(IV) complexes with new octahedral geometry that allows the attachment of two ligands with a specific targeting action to insure efficient delivery[29]. Through this work, we intended to demonstrate that azomethine and azomethine plus derivative Pt complexes can find stable geometry leading to strong adsorption energies onto (10,10) BNNTs sidewalls. Moreover, close analysis of the electronic properties in terms of density of states (DOS), electronic charge distribution and charge transfer in the case of the BNNT plus a drug molecule showed a weak modification of the drug molecule properties when functionalized on the nanotube.

DFT calculations

Several studies have shown that BNNT electronic properties are independent of nanotube diameter,[11, 12] contrarily to BNNT reactivity.[22, 23] Thus, we chose to represent the system of an armchair single-walled (10,10) BNNT by a finite-length cylindrical BN cage (i.e. diameter radius 13.94 Å, length 21.32 Å), consisting of 180 B and 180 N atoms. In order to avoid boundary effects, hydroxyl groups (–OH), consisting of 40 O and 40 H atoms, are introduced in the BNNT extremities, as depicted in Figure 1-a.[30] This allows treatment of any possible BNNT oxidation when solvated and avoids dangling bonds at their opened edge, which could dramatically modify their reactivity when the therapeutics attempt to encapsulate[16, 31]. We are aware of the modification of the BNNT electronic density due to functionalization. However, calculations on periodic nanotubes did not show any crucial modification of the lowest

binding energies inside the BNNT. Two molecules, azomethine and an amino derivative plus a Pt(IV) drug (Figures 1-b, 1-c), were taken into account to study the BNNT adsorption properties. The Pt(IV) drug alone could have been studied in order to compare its outer or inner interaction with BNNTs. Nevertheless, it is now commonly known that the chemical functionalization of nanocarriers and their dispersion in solvent can be obtained only using amino-derivative molecules. To be consistent with chemical interactions, a Pt(IV) drug was attached to amino derivatives in case of physical interactions. The BNNTs envisioned as nanocarriers had a length similar to the amino derivative plus the Pt(IV) drug at the beginning of optimisation.

The calculations employed projector augmented-wave (PAW) pseudopotentials as implemented in the VASP code (version 5.2.11) with a cutoff energy close to 400 eV corresponding to the standard precision level.[32, 33] The self-consistent cycles were stopped when variation of the total energy per unit cell and band structure energy were both less than 10^{-4} eV. A test with a higher cutoff did not modify the location and the conformation of the adsorbed molecules on the BNNT inner or outer surface. To ensure isolation of the total system, the size of the unit cell was approximately 50×50×60 $Å^3$, where the last number represented the length of the unit cell along the tube axis. Given the large unit cell, the Brillouin zone was sampled using a single k-point at the centre Γ.

Depending on the interactions between the adsorbate and the substrate, two adsorption processes were distinguished: chemisorption and physisorption. Chemisorption was due to the apparition of strong covalent bond while physisorption was dominated by the weak van der Waals (VdW) forces. It is now currently known that the Density Functional Theory (DFT) is well dedicated to the study of chemisorption, but cannot consider VdW interactions accurately. Besides, the local density approximation (LDA) overestimates the binding energy while the Generalized Gradient Approximation (GGA) underestimates them.[34, 35] For physisorption, the long range of interaction forces, such as VdW, cannot be neglected, showing the same magnitude as the chemical ones (acting mainly in chemisorption). They have been, for a long time, recognised as fundamental forces to obtain an accurate description of simple processes, such as the adsorption of molecules on solid surfaces, but also to demonstrate the stability of more complex systems, such as DNA and proteins.[36-39]

In this theoretical study, the exchange-correlation energy was described by the functional of Perdew, Burke, and Ernzerhof (PBE) based on the PW91 generalised gradient approximation (GGA) pseudopotentials and dispersion interactions were incorporated using the DFT-D2 method. Indeed, most of density functionals were unable to describe correctly the van der Waals (VdW) interactions resulting from dynamical correlations between fluctuating charge distributions. A pragmatic method to work around this problem was given by the DFT-D approach, which added a semi-empirical dispersion potential to the conventional Kohn-Sham DFT energy.

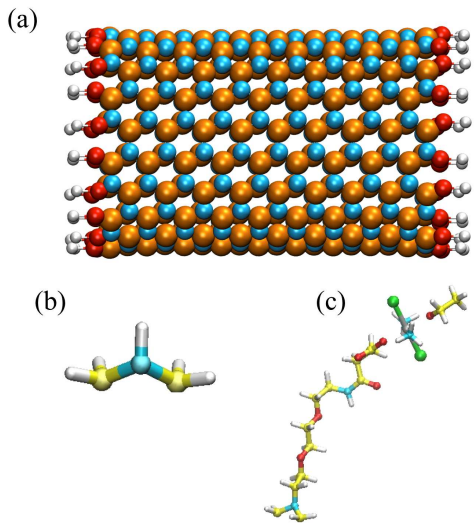

FIG. 1: Geometry of a) Single-walled (10,10) BNNT with hydroxyl groups (–OH) b) Azomethine (C_2H_5N) and c) Amino derivative plus a platinum complex.

However, this DFT-D scheme leads to predetermined and constant quantities unable to reproduce correctly the charges fluctuations no matter what its oxidation or hybridization state is. To circumvent this problem, the DFT-D2 method was implemented by Grimme[24-26] using simple pairwise force fields to treat van der Waals interactions optimised for several DFT functionals. Mostly because of the simplicity and low computational cost, this pairwise C_6/r_0^6 correction scheme was used in this work. Since the dispersion coefficient C_6 for platinum was not listed in Grimme's original paper[24-26], the value of 4.43 J nm^6 /mol was chosen to be consistent with the results by Bethune *et al.*[40] with a VdW radius for Pt (R_0) equal to 1.772 Å. All parameters are listed in Table I.

The electronic structures were relaxed until the components of the force on each atom were less than 0.01 $eV.Å^{-1}$. In order to take into account the dispersion of the different systems in aqueous solution, the permittivity was set accordingly (ε_{water}=80). The relaxed atomic positions of the systems under investigation and the local electronic densities of states were calculated. Noteworthy, one optimisation calculation performed on 32 cores needed about 14 days to converge.

Table 1: Parameters for Grimme's potential. Cutoff radius: 30.000 Å, global scaling factor: 0.750 Å, parameter d: 20.000 Å.

Atoms	C_6(J.nm^6/mol)	R_0(Å)
Pt	4.43	1.772
Cl	5.070	1.639
N	1.230	1.397
B	3.130	1.485
C	1.750	1.452
O	0.700	1.342
H	0.140	1.001

The adsorption energy (E_{ads}) of adsorbed molecules (Mol) on the inner (or outer surface) of the BNNT (Template) was derived from the energy difference between the different states of the system, namely, E_{ads}=E(Mol+Template)−E(Template)−E(Mol). A negative E_{ads} value denoted a more favourable interaction between the drug-nanotube systems. The charge transfers occurring in the covalent binding were analysed through a partial charge approach (i.e. valence electrons).[41-44]
In order to characterise the interaction between the molecule and the BNNT surface, the Bader scheme was used. According to this theory, the formation of a bond path is indicated by an accumulation of the electron density, ρ(r), between the nuclei of the bonded atoms, which is necessary for bond formation. Also, the Laplacian of ρ(r) (i.e. $\nabla^2\rho(r)$) marks the boundaries of regions where ρ(r) is locally above or below its average value in the vicinity of r. In the regions where $\nabla^2\rho(r)$ is negative, the electronic density is shared by both nuclei (shared interactions). Otherwise, the electrons are concentrated in each separated atomic basins and the interaction belongs to the closed-shell type.[42, 45, 46]

Results and discussion

Inner interaction

Firstly, the optimised geometry of the BNNTs with hydroxyl groups (–OH) was carried out. It showed an increase of the radius near the nanotube mouths with a slight decrease of the total length from 21.32 Å to 21.14 Å (Figure 2-a). The radius of the BNNTs at the centre of the nanotube (i.e. 13.94 Å) became 14.89 Å at both ends and this optimised geometry tended to a total energy of -3567.81 eV (Figure 2-b). This total energy was the reference (i.e. E(Template)) used during the determination of E_{ads}.

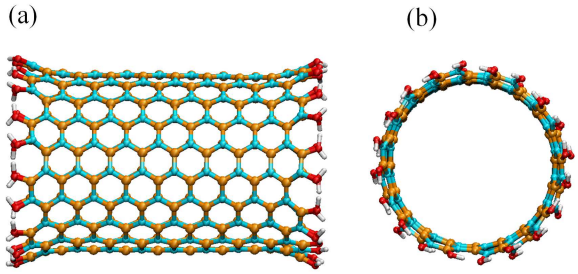

FIG. 2: Optimised geometry of single-walled (10,10) BNNT with hydroxyl groups (–OH) a) lateral view and b) perpendicular view.

To investigate how the azomethine molecule interacts with inner surface of the BNNTs, the molecule was placed in a symmetric position along its principal z-axis (Figure 3-a, Figure 3-b). The molecule was localised at an arbitrary distance and its position was optimised. The mean distance between the N atom of the molecule and the BNNT centre of mass, denoted as d, was calculated. Then, we progressively changed the position of the molecule and calculated the new optimised value of d to simulate the translation of the whole molecule from -16 Å to -3.4 Å inside the BNNT. For each distance, the whole structure was relaxed by allowing atom displacement to minimise the total energy. By subtracting both the total energy of the isolated tube and the energy of the molecule from the total energy of the combined structure after optimisation, we obtained the binding energy for the interacting system (Figure 3-c). It showed clearly that the interaction between the two molecules became attractive even for a distance equal to -5 Å from the BNNT centre of mass and the molecule stayed centred. At the entrance of the BNNT nanotube, the adsorption energy is -0.07 eV and converges through -0.11 eV inside. In addition to this central configuration, we placed the azomethine molecule closer to the inner wall surface of the (10,10) tube at a distance around 1.8 Å to highlight the role played by the hydroxyl groups. We relaxed the whole structure for different distances d, varying from -12.7 Å to -6.4 Å (Figure 3-d). It showed clearly that the interaction became more attractive than when the molecule was centred. Moreover, we observed a potential barrier located on the hydroxyl groups (red dashed line in Figure 3-d). Indeed, at the entrance of the BNNT nanotube, the adsorption energy was equal to -0.32 eV and decreased until -0.47 eV at -6.4 Å of the centre of mass, which represented the most stable adsorption site for this study.

Calculated electronic density of states (DOS) for this optimized position is presented in the bottom graph of Fig. 4. In the top and middle graphs of Fig. 4, the DOS for a (10,10) BNNT and for an isolated azomethine molecule are also represented, respectively, aligned to the same Fermi level (i.e 0.0 eV) as the bottom graph. It is obvious that the bottom graph is almost a superposition of the top and the middle graphs, with some discrepancies in the height of the DOS and a slight shift in energy levels of azomethine due to interaction. Moreover, we can identify in the gap of the BNNT-azomethine system, a peak at -1.0 eV corresponding to the two C atoms of the molecule with dangling bonds.

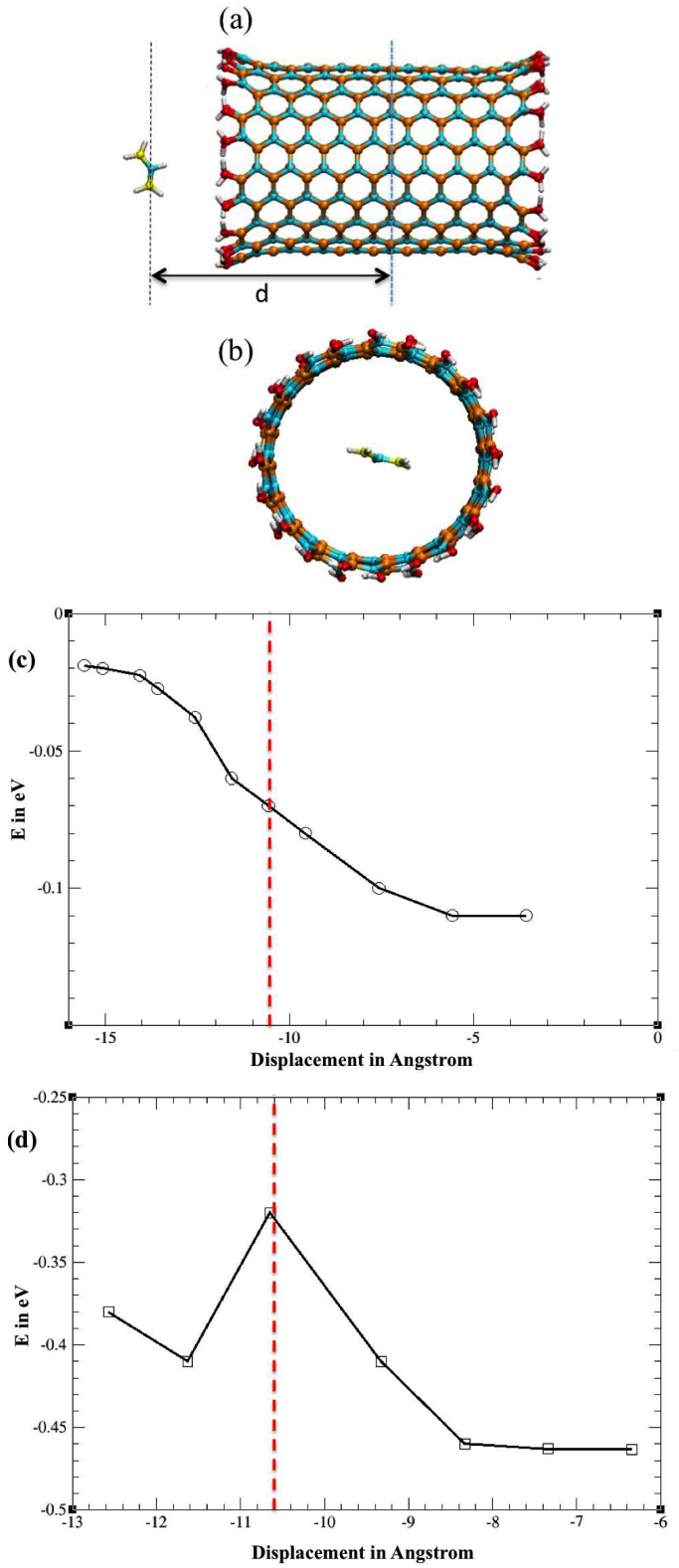

FIG. 3: Geometry of the azomethine-BNNT a) lateral view, the dashed blue line is the z-origin b) perpendicular view c) adsorption energy as a function of the distance between N atom of azomethine and BNNT centre of mass d) adsorption energy for azomethine molecule near the inner BNNT surface (i.e. 1.8 Å). Dashed red line corresponds to the nanotube hydroxyl mouth.

The electronic structure of each component of the combined structure was thus essentially intact despite encapsulation. Overall, the images confirmed the inert and non-reactive quality of BNNTs when azomethine encapsulation took place.

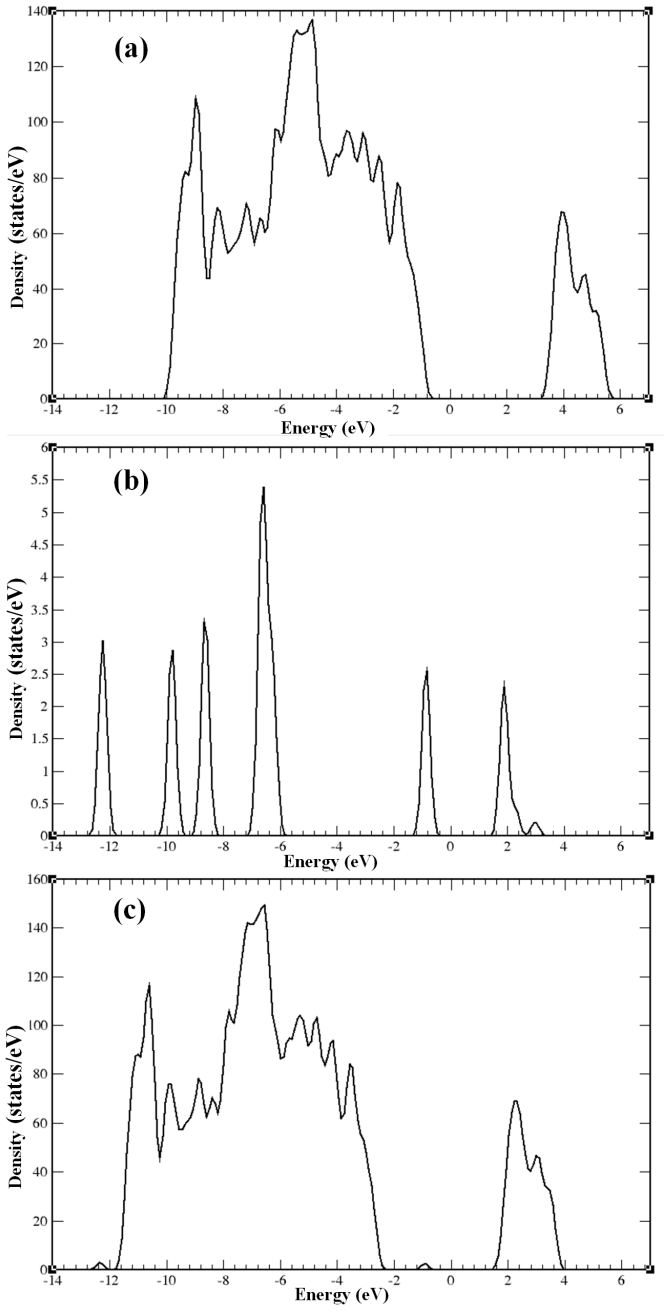

FIG. 4. DOS for a (10,10) BNNT (top graph), an isolated azomethine molecule (middle graph), and their combined structure (bottom graph). Fermi levels at E = 0 eV, were slightly different for BNNT, isolated azomethine molecule and interacting system.

We expanded our research to include an amino derivative plus a Pt(IV) drug. The molecule was placed in a symmetric position along its principal z-axis at a distance, denoted as d, defined as

the mean distance between the N atom of the amino derivative and BNNT centre of mass (Figure 5-a). The encapsulation went through relaxation and electronic structure calculations. The calculated binding energy for each distance d is depicted in Figure 5-b.

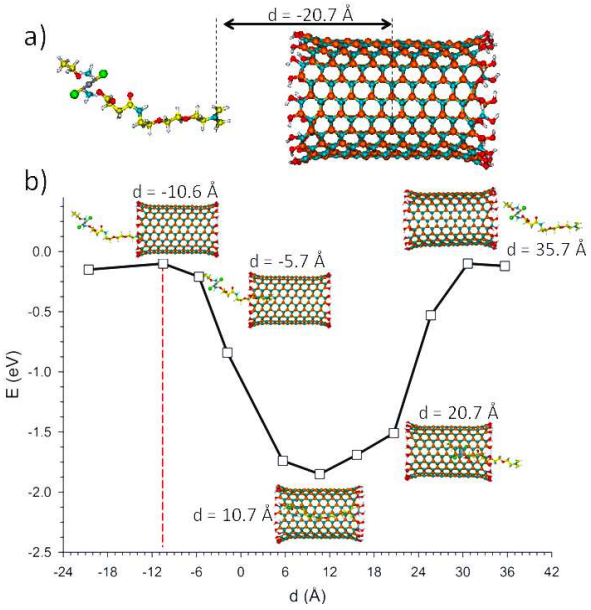

FIG. 5: Geometry of the amino derivative azomethine Pt drug-BNNT a) lateral view, the dashed line blue is the z-origin b) Adsorption energy as a function of the distance between N atom of amino derivative azomethine Pt drug and BNNT centre of mass. The dashed red line corresponds to the hydroxyl nanotube mouth. Some points are illustrated by the corresponding optimised geometry.

We observed that the adsorption energies for the amino derivative Pt drug were greater than in the case of azomethine adsorption with a minimum equal to -1.85 eV. The relaxation process forced the encapsulated molecule to reposition itself constantly near the BNNT centre thanks to the van der Waals interaction (Figure 5-b). The curve presented also a weak potential barrier at the hydroxyl mouth with energy equal to -0.11 eV. Moreover, the most stable configuration due to encapsulation did not show any chemical adsorption or bonding occurring between the molecules and the tube. Finally the exit of the molecule presents one small dissymmetry in the energy profile (Figure 5b) due to the asymmetry of the molecule during its displacement in the BNNT. In Figure 6, we present the DOS for the amino-derivative Pt drug encapsulated in BNNT for E_{ads} equal to -1.85 eV. The top graph represents the molecular DOS with the Fermi level at 0.0 eV, as for the bottom graph (Figure 6-a). This latter, which represents the encapsulation, is the superposition of the isolated systems with some discrepancies in the DOS height and a slight shift in the energy levels of the amino-derivative Pt drug due to interaction (Figure 6-b). Moreover, the gap of the BNNT-amino derivative Pt drug system was identified: three peaks at the Fermi level due to the molecule states. These entire results highlighted the inertness of the inner surface of BNNT, even with the encapsulated active drug.

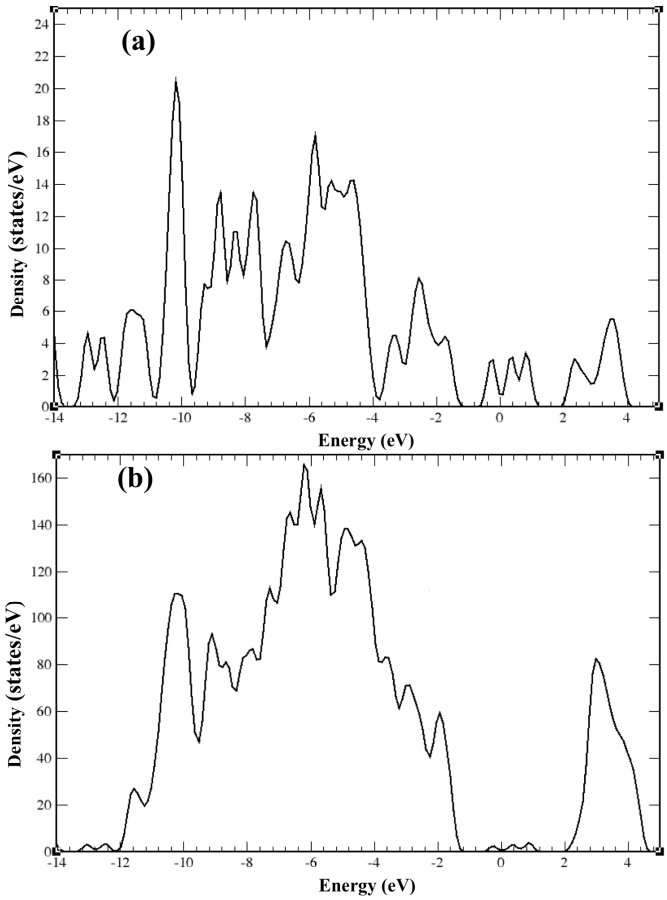

FIG. 6: DOS for an isolated amino-derivative Pt drug molecule (top graph), and the combined structure between the BNNT and the molecule (bottom graph). Fermi levels at E = 0 eV are slightly different for the isolated amino-derivative Pt drug and the interacting system.

Note that close inspection of the Grimme parameters showed that their values increased from a surface to a single atom. The same conclusion was obtained by S. Botti et al. when considering the passage from a cluster to an atom [47, 48]. To take into account such results, we decided to modify the C_6 coefficient for the Pt atom from 4.43, representing a bulk value, to 81.24 J.nm^6/mol, close to the value describing an isolated Pt atom. Optimisation of the interaction energies in the most stable site led to a slight modification (around 7%) of the adsorption energy from -1.85eV to -1.98eV.

Outer interaction

To investigate the interaction of the azomethine molecule on the outer surface of the BNNT, different orientations and adsorptions were envisioned. We considered the perpendicular or parallel orientation of the molecule with different sites: at the

centre of one B-N hexagon (hollow site), between two B-N bonds (bridge site) and on top of N and B atoms, respectively. The azomethine molecule was positioned at a mean distance of 1.5 Å from the BNNT outer surface relative to the C atom of azomethine. For each configuration, the whole structure was then relaxed by allowing all atoms to move in order to minimise the total energy. For the hollow and bridge sites, we observed, for all configurations, a strong repulsion between the BNNT and the molecule. The final distance between the azomethine molecule and the outer BNNT surface was around 3.1 Å. All atoms of the molecule were in the same plane. The adsorption energy was around -0.29 eV (Figure 7-a). Thus, there was no chemical adsorption or bonding occurrence between the molecules and the tube for these configurations. The stable site on outer surface was less favourable than the inner one due to the tube concavity.

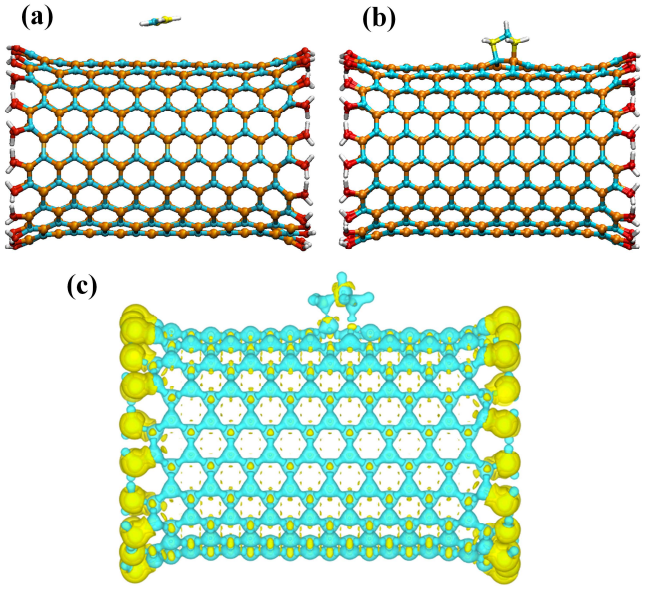

FIG. 7: Geometry of the azomethine-BNNT a) final relaxed position when starting initially atop a hollow site or bridge site b) Pentagon formation between azomethine and BNNT outer surface c) 3D representation view of the charge density Laplacian in the azomethine-BNNT pentagon formation. Colour scale varying from −7.5 to 7.5 *e* / Å^5 with blue for $\nabla^2\rho(r) < 0$ and yellow $\nabla^2\rho(r) > 0$.

On the contrary, on top of the N or B atom, the azomethine molecule interacted strongly with the BNNT. It tilted around the N or B atom and created a pentagon with the outer BNNT surface (Figure 7-b). We observed an apparent radial deformation of the BNNT, where B and N atoms pulled outwards to the BNNT surface. We reported similar deformation, which lead to a quasi-regular pentagon due to hybridisation in covalently functionalized carbon nanotubes.[49] To the best of our knowledge, this structural deformation can be attributed to the change from sp^2 to sp^3 hybridisation on the B and N atoms with the C atoms of azomethine, respectively. In this configuration, the B–C and N–C bond lengths were equal to 1.63, and 1.55 Å, respectively. Besides, the adsorption energy of azomethine on the BNNT outer surface in this configuration was equal to −5.94 eV for two bonds. While strong, this bond formation remained extremely site selective since the azomethine molecule needed to attack the BNNT surface on specific sites. Analysis of the Laplacian electronic density corroborated the fact that cycloaddition took place. In Figure 7-c, 3D representation of the azomethine-BNNT Laplacian is reported with colour scale varying from −7.5 to 7.5 *e* / Å^5 with blue for $\nabla^2\rho(r) < 0$ and yellow for $\nabla^2\rho(r) > 0$. We observed that C–N and C–B bonds responsible for the azomethine and the BNNT outer surface link led to negative $\nabla^2\rho(r)$ values. This is typically the case where the electronic density is shared by both nuclei (i.e. shared covalent or ionic interactions).

We next expanded our study to the amino-derivative plus Pt(IV) drug on the outer surface of the BNNT. Due to the aforementioned covalent adsorption of azomethine, we considered adsorption on top of N and B atoms only. Relaxation simulations showed strong interaction between the molecule and the BNNT. We observed the same behaviour as for azomethine with an apparent radial deformation of the BNNT surface (Figure 8-a). In this configuration, the B–C and N–C bond lengths between the BNNT surface and the amino-derivative plus Pt(IV) drug molecule were equal to 1.63, and 1.54 Å, respectively. Besides, the adsorption energy of the molecule on the BNNT outer surface in this configuration was equal to −6.04 eV for two bonds. In Figure 8-b, 3D representation of the amino-derivative plus Pt(IV) molecule-BNNT Laplacian was reported. The same characteristics as for azomethine were obtained since $\nabla^2\rho(r)$ was negative for the two newly created bonds. The electronic density was thus shared by both nuclei, i.e. shared covalent or ionic interactions. All these results showed that cycloaddition took place for azomethine as well as for the amino-derivative plus Pt(IV) drug.

For the drug delivery purposes, one of the main questions concerned the electronic and the conformational stability of the therapeutic agent covalently attached to the BNNT. Initially, we determined the covalent Bader's charges for Pt, Cl and N atoms of the Pt(IV) agent. The different results are shown in Table 2.

Comparison with the amino derivative Pt(IV) agent drug alone showed a charge loss of 0.71e on the Pt atom when associated with the amino-derivative functional group. When the molecule was covalently attached to the BNNT surface, we observed a slight diminution of the Pt charge equal to 0.07e. On the contrary, a slight increase of the charge on the Cl atoms (i.e. 0.05e) and the two NH_3 (i.e 0.02 e) around the Pt atom was obtained, which compensated for the decrease on the Pt atom. The remaining atoms constituting the drug were not implied in the electronic transfers.

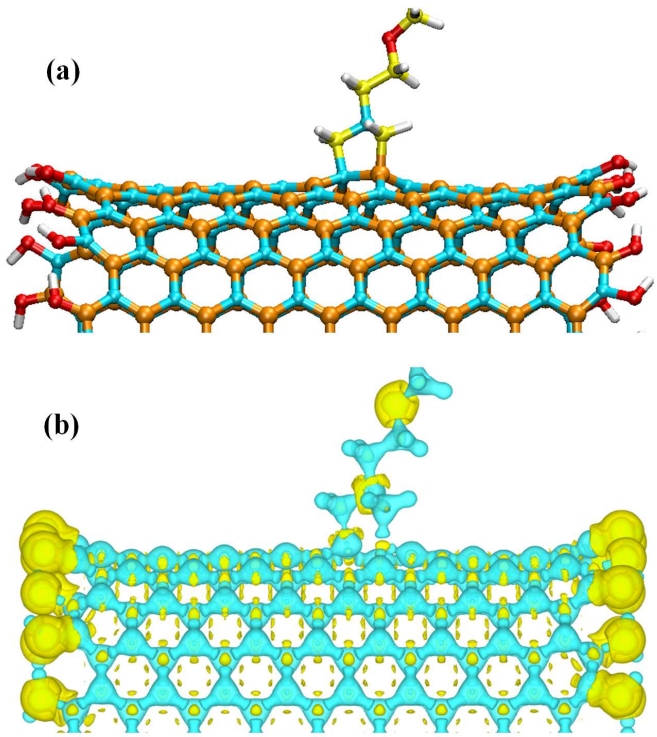

FIG. 8: Geometry of the azomethine-derivative plus Pt(IV) drug -BNNT a) zoom in the pentagon relaxed conformation b) 3D representation view of the charge density Laplacian, azomethine-BNNT, pentagon formation. Colour scale varying from −7.5 to 7.5 e / Å^5 with blue for $\nabla^2\rho(r) < 0$ and yellow $\nabla^2\rho(r) > 0$.

Table 2: Covalent Bader's charges (in elementary charge unit) located on the Pt, Cl and N atoms of the transplatin drug alone or linked on amino-derivative groups and on BNNT OH-ended nanotube.

	Transplatin	Transplatin+amino derivative	Transplatin+amino derivative on BNNT
Pt	9.32	8.61	8.54
Cl	7.56	7.45	7.49
	7.56	7.48	7.49
NH_3	7.76	7.71	7.72
	7.78	7.70	7.73

Conclusion

Using DFT-D2 calculations, we investigated interactions between single wall (10,10) boron nitride nanotubes and different molecules: azomethine (C_2H_5N) and an amino-derivative chain ending with an anticancer agent (Pt(IV) complex. Optimisation of the (10,10) BNNT-azomethine and BNNT-amino derivative systems was performed by considering different geometrical configurations on the inner and outer surfaces of the nanotube. Simulation results showed that only physisorption can occur between the molecules and the inner surface of the BNNT. Interaction between molecules and the outer BNNT surface are more complex. Adsorption on the hollow or bridge site highlighted a weaker interaction (i.e. physisorption) than in the inner surface. On the contrary, adsorption of the BNNT on B or N atoms led to strong chemisorption for the two molecules studied in this paper. The attachment of azomethine plus a subsequent drug, such as a Pt(IV) complex, did not perturb the cycloaddition process. Moreover, all theoretical results showed that the therapeutic agent complex was slightly affected when it was attached onto BNNTs. At that point, if one considers that platinum complexes are active anticancer drugs due to their strong electrophilic character with respect to DNA, the attachment onto the BNNT did not significantly change their activity. These results provide an interesting basis for the role of BNNT as an inert nanocarrier of the active platinum drug molecule towards side cells. The present results are expected to provide useful guidance for the potential application of BNNT-based materials in medicine therapy.

Acknowledgement

The calculations were carried out with the supercomputer regional facility Mésocentre of the University of Franche-Comté.

References

1. M. Ferrari, *Nat Rev Cancer*, 2005, **5**, 161-171.
2. K. K. Jain, *Clinical Chemistry*, 2007, **53**, 2002-2009.
3. P. S. Kim, S. Djazayeri and R. Zeineldin, *Gynecologic Oncology*, 2011, **120**, 393-403.
4. K. Kostarelos, A. Bianco and M. Prato, *Nat Nano*, 2009, **4**, 627-633.
5. S. H. D. P. Lacerda, J. J. Park, C. Meuse, D. Pristinski, M. L. Becker, A. Karim and J. F. Douglas, *ACS Nano*, 2009, **4**, 365-379.
6. D. A. LaVan, T. McGuire and R. Langer, *Nat Biotech*, 2003, **21**, 1184-1191.
7. R. A. Rippel and A. M. Seifalian, *Journal of Nanoscience and Nanotechnology*, 2011, **11**, 3740-3748.
8. M. Wang and M. Thanou, *Pharmacological Research*, 2010, **62**, 90-99.
9. A. Bianco, K. Kostarelos and M. Prato, *Current Opinion in Chemical Biology*, 2005, **9**, 674-679.
10. C. L. Lay, J. Liu and Y. Liu, *Expert Review of Medical Devices*, 2011, **8**, 561-566.
11. X. Blase, A. Rubio, S. Louie and M. Cohen, *Europhys Lett* 1994, **28**, 335–340.
12. A. Rubio, J. Corkill and C. ML, *Phys Rev B* 1994, **49**, 5081–5084.

13. X. Chen, P. Wu, M. Rousseas, D. Okawa, Z. Gartner, A. Zettl and C. Bertozzi, *J Am Chem Soc*, 2009, **131**, 890–891.
14. C. Zhi, Y. Bando, C. Tang, Q. Huang and D. Golberg, *J Mater Chem* 2008, **18**, 3900–3908.
15. G. Gou, B. Pan and L. Shi, *ACS Nano* 2010, **4**, 1313–1320.
16. W. Wang, Y. Bando, C. Zhi, W. Fu, E. Wang and D. Golberg, *J Am Chem Soc* 2008, **130**, 8144–8145.
17. C. Zhi, Y. Bando, C. Tang and G. D, *Phys. Rev. B* 2006, **74**, 153413–153414.
18. B. Akdim, S. Kim, R. Naik, B. Maruyama, M. Pender and R. Pachter, *Nanotechnology* 2009, **20**, 1–8.
19. Z. Gao, C. Zhi, Y. Bando, D. Golberg and T. Serizawa, *ACS Appl Mater Interfaces*, 2011, **3**, 627–632.
20. S. Mukhopadhyay, S. Gowtham, R. Scheicher, R. Pandey and S. Karna, *Nanotechnology* 2010, **21**, 1–6.
21. J. Zhao and Y. Ding, *Diam Relat Mater* 2010, **19**, 1073–1077.
22. R. Batista, A. B de Oliveira and D. Rocco, *J. Phys.: Condens. Matter* 2010, **22**, 355302-355307.
23. Y. Li, Z. Zhou and J. Zhao, *J. Chem. Phys.* , 2007, **127**, 184705
24. S. Grimme, *Journal of Computational Chemistry*, 2004, **25**, 1463-1473.
25. S. Grimme, *Journal of Computational Chemistry*, 2006, **27**, 1787-1799.
26. S. Grimme, J. Antony, T. Schwabe and C. Muck-Lichtenfeld, *Organic & Biomolecular Chemistry*, 2007, **5**, 741-758.
27. S. Dhar, Z. Liu, J. r. Thomale, H. Dai and S. J. Lippard, *Journal of the American Chemical Society*, 2008, **130**, 11467-11476.
28. S. J. Lippard, *Abstracts of Papers of the American Chemical Society*, 2009, **237**, 613-613.
29. S. D. Brown, P. Nativo, J. Smith, D. Stirling, P. R. Edwards, B. Venugopal, D. J. Flint, J. A. Plumb, D. Graham and N. J. Wheate, *J Am Chem Soc.* , 2010, **132**, 4678–4684.
30. C. Zhi, Y. Bando, T. Terao, C. Tang, H. Kuwahara and D. Golberg, *Chemistry* 2009, **4**, 1536–1540.
31. J. Zhao and Y. Ding, *Nanotechnology*, 2009, **20**, 085704.
32. G. Kresse and J. Furthmuller, *Physical Review B*, 1996, **54**, 11169-11186.
33. G. Kresse and J. Hafner, *Physical Review B*, 1993, **47**, 558-561.
34. J. P. Perdew, K. Burke and M. Ernzerhof, *Physical Review Letters*, 1996, **77**, 3865-3868.
35. P. Sony, P. Puschnig, D. Nabok and C. Ambrosch-Draxl, *Phys. Rev. Lett.* , 2007, **99**, 176401- 176404.
36. J. Carrasco, B. Santra, J. Klimes and A. Michaelides, *Phys. Rev. Lett* 2011, **106**, 026101
37. S. Chakarova-Kack, E. Schroder, B. Lundqvist and D. Langreth, *Phys. Rev. Lett.* , 2006, **96**, 146107.
38. V. Cooper, T. Thonhauser, A. Puzder, E. Schroder, B. Lundqvist and D. Langreth, *J. Am. Chem. Soc.* , 2008, **130**, 1304.
39. K. Johnston, J. Kleis, B. Lundqvist and R. Nieminen, *Phys. Rev. B* 2008, **77**, 121404(R).
40. D. S. Bethune, J. A. Barker and C. T. Rettner, *The Journal of Chemical Physics*, 1990, **92**, 6847-6854.
41. R. Bader and G. Jones, *Can. J. Chem.* , 1961, **39**, 1253-1265
42. G. Henkelman, A. Arnaldsson and H. JÃ³nsson, *Computational Materials Science*, 2006, **36**, 354-360.
43. C. F. Matta and R. Boyd, *The Quantum Theory of Atoms in Molecules* Wiley, 2007.
44. W. Tang, E. Sanville and G. Henkelman, *J. Phys.: Condens. Matter* 2009, **21**, 084204-084207
45. R. Bader, *Pure Appl. Chem.* , 1988, **60**, 145-155.
46. R. Bader, *Chem. Rev.* , 1991, **91**, 893-928.
47. S. Botti, A. Castro, X. Andrade, A. Rubio and M. A. L. Marques, *Phys Rev B*, 2008, **78**, 035333.
48. M. T. Nguyen, C. A. Pignedoli, M. Treier, R. Fasel and D. Passerone, *Phys Chem. Chem. Phys.*, 2010, **12**, 992.
49. S. Kraszewski, E. Duverger, C. Ramseyer and F. Picaud, *J. Chem. Phys.* , 2013, **139**, 174704-174711.